Efficacy and mechanism of nano-biochar supported TiO$_2$ in removing dichloroacetic acid from swimming pools

Xin Shu[1], Xunlan Liu[2]

[1]Ministry of Sports, Capital University of Economics and Business. Beijing, China.

[2]Rehabilitation Center, National Sports Training Center. Beijing, China.

e-mail: shuxin810404@163.com, liuxunlan139@163.com

ABSTRACT

This study synthesized novel nano-biochar supported TiO$_2$ composites using various methods and biochar/TiO$_2$ ratios to effectively remove dichloroacetic acid (DCA) from swimming pool water. The hydrothermally prepared HBT-5 composite with 5 wt% biochar exhibited the highest photocatalytic activity, degrading 92.5% of DCA within 180 min under UV-vis light irradiation, outperforming pure TiO$_2$ and HBT-1. Comprehensive characterization confirmed the strong interaction and synergistic effects between biochar and TiO$_2$, attributing the enhanced performance to high surface area, pore volume, interfacial Ti-O-C bonding, visible light absorption, efficient charge separation, and N and O heteroatoms in biochar. The photocatalyst showed excellent reusability, maintaining 87.3% of its initial activity after three cycles. This work provides insights into designing biochar-based photocatalysts for water purification, benefiting public health and environmental protection.

Keywords: Photocatalytic degradation; Haloacetic acid; Water treatment; Hydrothermal synthesis; Synergistic effect.

1. INTRODUCTION

Swimming pools are widely utilized aquatic facilities that serve millions of users globally for recreational and athletic purposes. Disinfectants such as chlorine are routinely added to pool water to inactivate harmful pathogens and prevent waterborne diseases [1, 2]. While chlorination is effective in controlling microbial growth, it can also lead to the formation of disinfection byproducts (DBPs) when chlorine reacts with organic matter present in the water [3]. Dichloroacetic acid (DCA) is one of the most commonly detected DBPs in chlorinated swimming pools [4]. DCA is a haloacetic acid that has been classified as a potential human carcinogen by the International Agency for Research on Cancer. Exposure to DCA in swimming pools can occur through ingestion, inhalation, and dermal absorption, raising concerns about its health risks, particularly for frequent swimmers and pool workers [5].

Conventional water treatment methods such as filtration and adsorption have limited efficacy in removing DCA from swimming pools [4, 6]. Advanced oxidation processes (AOPs) have emerged as promising technologies for the degradation of recalcitrant organic pollutants like DCA. AOPs involve the generation of highly reactive hydroxyl radicals (·OH) that can mineralize organic contaminants into harmless end products such as CO$_2$ and water [7]. Among various AOPs, heterogeneous photocatalysis using titanium dioxide (TiO$_2$) has attracted significant attention due to its high efficiency, stability, and eco-friendliness [8, 9]. When irradiated with light of appropriate wavelength, TiO$_2$ generates electron-hole pairs that can initiate redox reactions, leading to the formation of ·OH and other reactive oxygen species capable of degrading organic pollutants [10]. Despite its advantages, TiO$_2$ photocatalysis suffers from certain limitations that hinder its practical application. TiO$_2$ has a wide band gap (3.2 eV for anatase phase) that restricts its photoactivation to the UV region, which comprises only 4-5% of the solar spectrum. Moreover, the high recombination rate of photogenerated electron-hole pairs in TiO$_2$ reduces its quantum efficiency [11, 12]. To overcome these drawbacks, various strategies have been explored, such as doping TiO$_2$ with metal/non-metal elements, coupling with other semiconductors, and immobilizing on carbonaceous supports [13–15]. In particular, the use of biochar as a support for TiO$_2$ has gained increasing interest in recent years. Biochar is a carbon-rich material produced by the pyrolysis of biomass waste under oxygen-limited conditions [16–18]. It has a highly porous structure, large specific surface

area, and abundant surface functional groups, making it an excellent adsorbent for various pollutants. When used as a support for TiO$_2$, biochar can enhance its photocatalytic activity through several mechanisms [19, 20]. Firstly, the porous structure of biochar provides a high dispersion of TiO$_2$ nanoparticles, increasing their available surface area for photocatalytic reactions [15]. Secondly, the strong adsorption capacity of biochar can concentrate pollutants near the TiO$_2$ surface, facilitating their degradation [21]. Thirdly, the graphitic carbon in biochar can act as an electron acceptor, reducing the recombination of photogenerated charge carriers in TiO$_2$ and improving its quantum efficiency [22]. Furthermore, heteroatoms such as N and O present in biochar can narrow the band gap of TiO$_2$, extending its light absorption into the visible region [23, 24].

Several studies have reported the enhanced photocatalytic activity of biochar-supported TiO$_2$ for the degradation of various organic pollutants [25–27]. However, the application of this composite material for the removal of DCA from swimming pool water has not been extensively explored. Moreover, the influence of synthesis methods and biochar/TiO$_2$ ratios on the photocatalytic performance remains to be systematically investigated. Therefore, the objectives of this study are: (1) to synthesize novel nano-biochar supported TiO$_2$ composites using different methods (hydrothermal, solvothermal, and mechanical) and biochar/TiO$_2$ ratios (1−10%); (2) to characterize the physicochemical properties of the composites using various techniques; (3) to evaluate their photocatalytic activity for DCA degradation under UV-vis light irradiation; and (4) to elucidate the mechanism of enhanced photocatalytic performance in the biochar-TiO$_2$ system. The novelty of this work lies in the development of highly efficient and sustainable biochar-based photocatalysts for the removal of a specific DBP in swimming pools, which has not been reported before. The findings of this study are expected to provide new insights into the design and application of biochar-supported photocatalysts for water purification, with potential benefits for public health and environmental protection.

2. MATERIALS AND METHODS

All chemicals used in this study were of analytical grade and used without further purification. Titanium dioxide (TiO$_2$, anatase, 99.8% purity, 25 nm average particle size) was purchased from Shanghai Macklin Biochemical Co., Ltd. Dichloroacetic acid (DCA, 99%) and humic acid (HA, technical grade) were obtained from Beijing Solarbio Science & Technology Co., Ltd. Peanut shells were collected from a local farm in Shandong Province, China. Ethanol (99.7%), acetic acid (99.5%), and other solvents were procured from Sinopharm Chemical Reagent Co., Ltd.

Peanut shell biochar was prepared by slow pyrolysis in a tube furnace (OTF-1200X, Hefei Kejing Materials Technology Co., Ltd.). The peanut shells were washed thoroughly with deionized water to remove dirt and impurities, dried at 105 °C for 24 h, and then ground and sieved to obtain particles of 0.5−1 mm size. The peanut shell particles were placed in a ceramic boat and heated in the tube furnace under a nitrogen flow of 500 mL/min. The pyrolysis temperature was raised from room temperature to 700 °C at a heating rate of 10 °C/min and maintained at 700 °C for 2 h. After cooling down to room temperature, the biochar was collected, ground, and sieved through a 100-mesh sieve to obtain a fine biochar powder.

Biochar-TiO$_2$ composites were synthesized using three different methods: hydrothermal, solvothermal, and mechanical mixing. For the hydrothermal method, a calculated amount of biochar (1, 5, or 10 wt% relative to TiO$_2$) was dispersed in 50 mL of deionized water by sonication for 30 min. Then, 1 g of TiO$_2$ was added to the biochar suspension and stirred magnetically for 2 h to obtain a homogeneous mixture. The mixture was transferred to a 100 mL Teflon-lined stainless-steel autoclave and heated at 180 °C for 12 h. After cooling naturally to room temperature, the resulting composite was collected by centrifugation, washed with deionized water and ethanol, and dried at 80 °C for 12 h. The samples were denoted as HBT-x, where x represents the biochar content (1, 5, or 10 wt%).

For the solvothermal method, the procedure was similar to the hydrothermal method, except that ethanol was used as the solvent instead of water. The biochar-TiO$_2$ suspension in ethanol was stirred for 2 h, transferred to the autoclave, and heated at 180 °C for 12 h. The resulting composites were labeled as SBT-x. In the mechanical mixing method, biochar and TiO$_2$ powders were mixed in the desired proportions (1, 5, or 10 wt% biochar) and ground in an agate mortar for 30 min to achieve a uniform mixture. The samples were named as MBT-x. For comparison, pure TiO$_2$ was also treated under the same hydrothermal and solvothermal conditions without the addition of biochar.

The photocatalytic activity of the prepared samples was evaluated by the degradation of DCA under UV-vis light irradiation. The experiments were carried out in a photochemical reactor (XPA-7, Xujiang Electromechanical Plant) equipped with a 300 W xenon lamp (CEL-HXF300, Beijing China Education Au-light Co., Ltd.) as the light source. The light intensity was measured by a radiometer (FZ-A, Photoelectric Instrument Factory of Beijing Normal University) and maintained at 100 mW/cm^2. A quartz tube containing 50 mL of DCA

solution (20 mg/L) and 50 mg of photocatalyst was placed in the center of the reactor. The suspension was magnetically stirred in the dark for 30 min to establish the adsorption-desorption equilibrium. Then, the xenon lamp was turned on to initiate the photocatalytic reaction. At given time intervals, 2 mL of the suspension was sampled, centrifuged, and filtered through a 0.22 μm PTFE membrane for analysis.

The concentration of DCA was determined by ion chromatography (IC) using a Dionex ICS-1100 system equipped with an AS11-HC anion-exchange column and a conductivity detector. The mobile phase was 30 mM KOH at a flow rate of 1.0 mL/min, and the injection volume was 25 μL. The total organic carbon (TOC) content was measured using a Shimadzu TOC-LCPH analyzer to evaluate the mineralization degree of DCA. The photocatalytic removal rate of DCA was calculated using the following equation:

$$\text{DCA removal rate (\%)} = (1 - C_t/C_0) \times 100\%$$

where C_0 is the initial concentration of DCA, and C_t is the concentration at time t.

The kinetics of DCA degradation were analyzed using the pseudo-first-order model, which is commonly applied to photocatalytic degradation processes. The model is expressed as:

$$\ln(C_0/C\_t) = kt$$

where C_0 is the initial concentration of DCA, C_t is the concentration at time t, k is the pseudo-first-order rate constant (min^{-1}), and t is the reaction time (min). The rate constant k was determined from the slope of the linear plot of $\ln(C_0/C\_t)$ versus t. The coefficient of determination (R^2) was calculated to assess the goodness of fit of the kinetic model to the experimental data. These kinetic parameters provide a quantitative measure of the photocatalytic efficiency of the different materials tested.

The reusability of the photocatalyst was tested by recycling the used HBT-5 sample for three consecutive runs. After each run, the photocatalyst was collected by centrifugation, washed with deionized water and ethanol, dried at 80 °C, and reused for the next run under the same conditions. All experiments were performed in triplicate, and the average values were reported. Control experiments were also conducted to assess the photolysis of DCA without a photocatalyst and the adsorption of DCA on the photocatalyst in the dark.

3. RESULTS AND DISCUSSION

3.1. Characterization of biochar-TiO$_2$ composites

The successful formation of biochar-TiO$_2$ composites was confirmed by various characterization techniques. Figure 1 presents the XRD patterns of pure TiO$_2$, biochar, and biochar-TiO$_2$ composites prepared by different methods. Pure TiO$_2$ exhibited characteristic diffraction peaks at 2θ = 25.3°, 37.8°, 48.0°, 53.9°, 55.1°, 62.7°, 68.8°, 70.3°, and 75.0°, which were indexed to the (101), (004), (200), (105), (211), (204), (116), (220), and

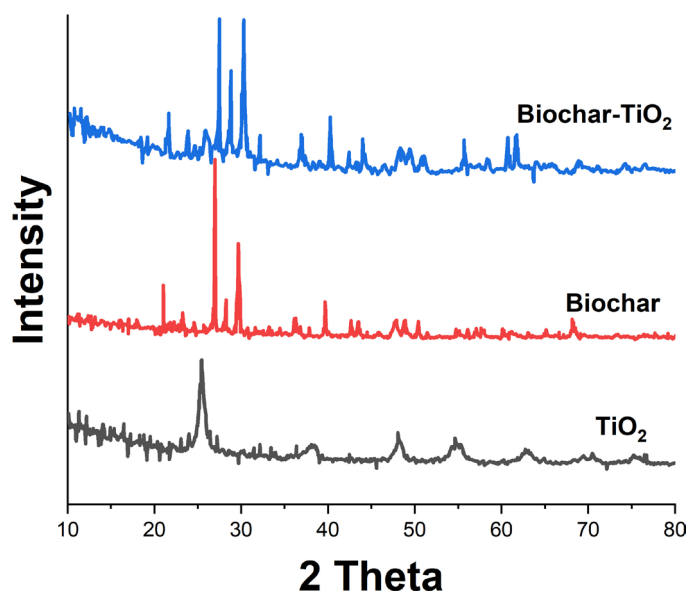**Figure 1:** XRD patterns of pure TiO$_2$, biochar, and biochar-TiO$_2$ composites prepared by different methods.

(215) planes of anatase TiO_2 (JCPDS No. 21-1272) [16]. Biochar showed a broad peak at around 23.0° and a weak peak at 43.5°, corresponding to the (002) and (100) planes of graphitic carbon [28], respectively. All biochar-TiO_2 composites displayed diffraction peaks of anatase TiO_2 without any impurity phases, indicating that the incorporation of biochar did not alter the crystal structure of TiO_2 [29]. However, the characteristic peaks of biochar were not clearly observed in the composites, likely due to its low content and high dispersion on the TiO_2 surface.

FTIR spectra were obtained to identify the functional groups present in the samples. As shown in Figure 2, pure TiO_2 exhibited a strong absorption band at 400–800 cm^{-1}, which was attributed to the stretching vibrations of Ti-O and Ti-O-Ti bonds in the TiO_2 lattice [30]. Biochar displayed several absorption bands at 3400, 1600, and 1100 cm^{-1}, corresponding to the stretching vibrations of O-H, C=C, and C-O groups [31], respectively. The biochar-TiO_2 composites showed characteristic bands of both TiO_2 and biochar, confirming the successful integration of the two components [32]. Notably, the intensity of the O-H and C-O bands decreased in the composites, suggesting the formation of Ti-O-C bonds between biochar and TiO_2.
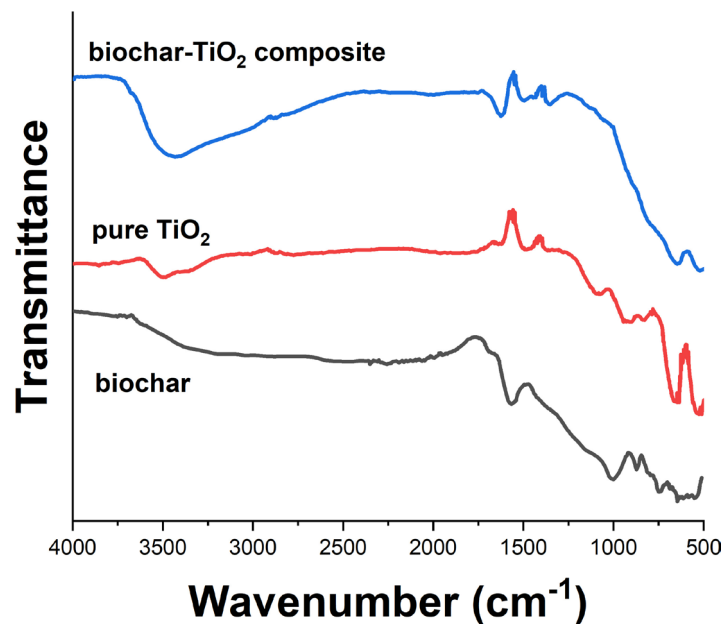

Figure 2: FTIR spectra of pure TiO_2, biochar, and biochar-TiO_2 composites prepared by different methods.
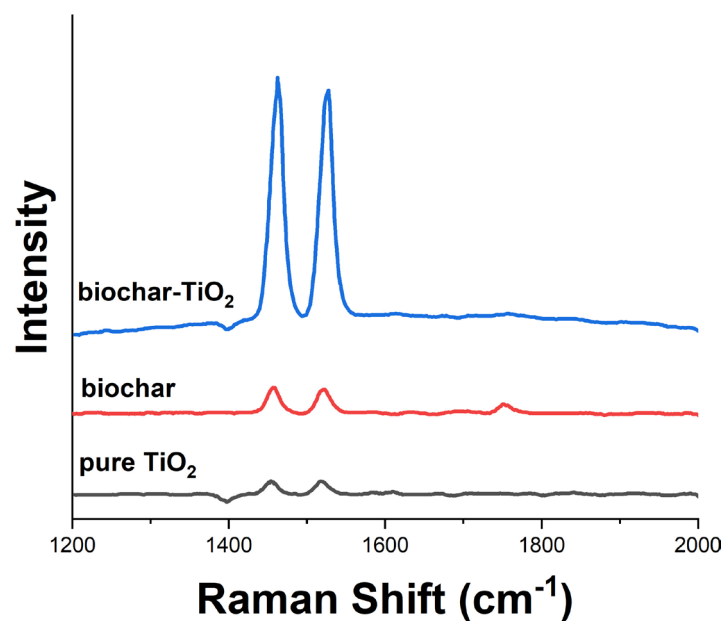

Figure 3: Raman spectra of pure TiO_2, biochar, and biochar-TiO_2 composites prepared by different methods.

Raman spectroscopy was employed to further investigate the structural features of the samples. In Figure 3, biochar exhibited two prominent bands at 1355 and 1598 cm^{-1}, known as the D band (disordered carbon) and G band (graphitic carbon), respectively. The biochar-TiO$_2$ composites displayed Raman bands of both TiO$_2$ and biochar, further confirming their successful combination [33]. The I_D/I_G ratio, which reflects the degree of graphitization, was calculated to be 0.95 for biochar and increased to 1.05−1.15 for the composites, indicating a slight decrease in the graphitization degree due to the interaction with TiO$_2$.

The morphology and microstructure of the samples were examined by SEM. SEM images (Figure 4) revealed that pure TiO$_2$ consisted of spherical nanoparticles with an average size of 20−30 nm, while biochar exhibited an irregular porous structure with a rough surface. The biochar-TiO$_2$ composites showed a uniform distribution of TiO$_2$ nanoparticles on the biochar surface, with no apparent aggregation.

The surface chemical composition and states of the samples were analyzed by XPS. The survey spectra (Figure 5a) indicated the presence of C, O, and Ti in the biochar-TiO$_2$ composites. The high-resolution C1s spectra (Figure 5b) of composites were deconvoluted into three peaks at 284.6, 285.7, and 288.5 eV, assigned to C-C/C=C, C-O, and C=O bonds [34], respectively. In the composites, the relative intensity of the C-O peak increased, and a new peak appeared at 283.5 eV, which was attributed to the Ti-O-C bond [35]. The O1s spectra (Figure 5c) of the composites showed two peaks at 530.2 and 532.0 eV, corresponding to Ti-O and C-O bonds, respectively. The Ti2p spectra (Figure 5d) of the composites displayed two peaks at 458.8 and 464.5 eV, assigned
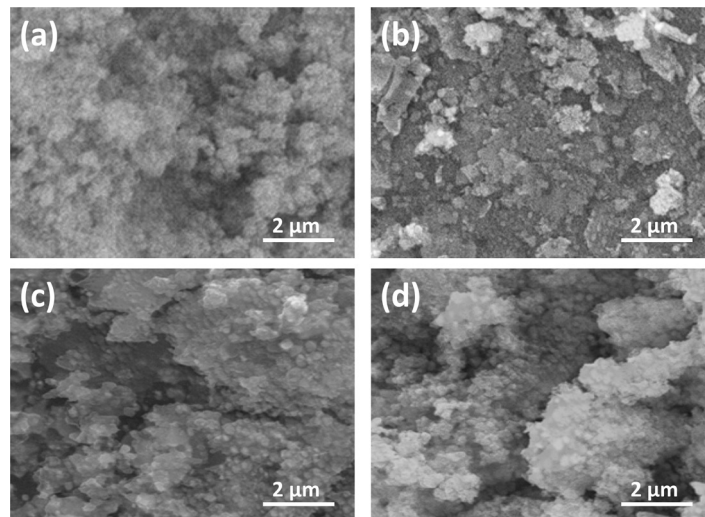

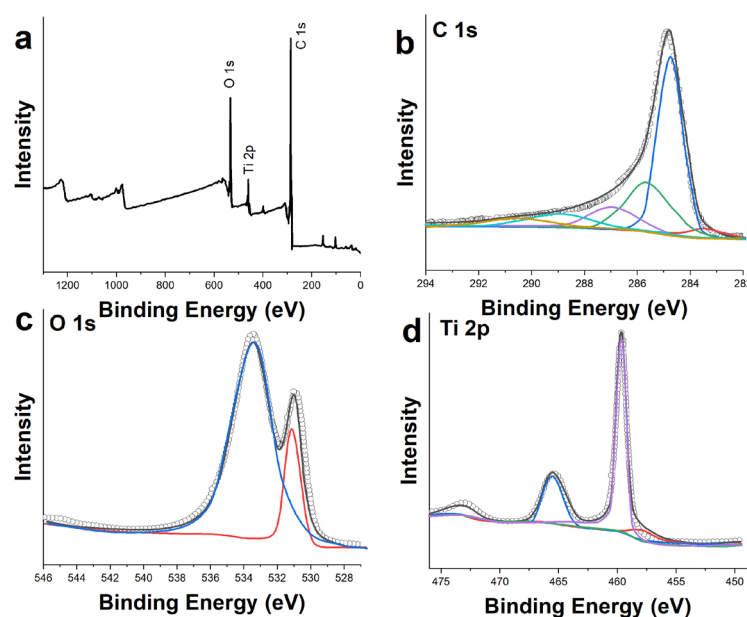**Figure 4:** SEM images of (a) pure TiO$_2$, (b) biochar, (c) HBT-1, (d) HBT-5, and (e) HBT-10.

Figure 5: XPS spectra of HBT-5: (a) survey, (b) C1s, (c) O1s, and (d) Ti2p.

to Ti $2p_{3/2}$ and Ti $2p_{1/2}$ of Ti^{4+} species [36], respectively, with a spin-orbit splitting of 5.7 eV. These results confirmed the chemical bonding between biochar and TiO_2 through Ti-O-C linkages.

The optical properties of the samples were investigated by UV-vis DRS. As shown in Figure 6a, pure TiO_2 exhibited strong absorption in the UV region (< 400 nm) due to its wide band gap, while biochar showed broad absorption in the visible region (400–800 nm) arising from its conjugated aromatic structure [37]. The biochar-TiO_2 composites displayed enhanced absorption in both UV and visible regions compared to pure TiO_2, indicating the sensitization effect of biochar. The band gap energies of the samples were estimated from the Tauc plots (Figure 6b) to be 3.11, 3.13, 3.15, and 3.19 eV for pure TiO_2, HBT-1, HBT-5, and HBT-10, respectively. The narrowing of the band gap with increasing biochar content suggests the formation of an interfacial Ti-O-C bond, which could facilitate charge transfer and extend the light absorption range [38].

The textural properties of the samples were evaluated by nitrogen adsorption-desorption measurements. The isotherm curves (Figure 7a) of all samples exhibited type IV isotherms with H3 hysteresis loops, characteristic of mesoporous materials. Pure TiO_2 had a relatively low surface area of 50.2 m^2/g, while biochar possessed a high surface area of 420.5 m^2/g and a large pore volume of 0.35 cm^3/g. The biochar-TiO_2 composites showed increased surface areas and pore volumes compared to pure TiO_2, reaching 125.8 m^2/g and 0.28 cm^3/g for HBT-5, respectively. The pore size distribution curves (Figure 7b) revealed that biochar had a wide range of pores from micro- to macropores, while the composites exhibited a narrower distribution centered at 3–4 nm, indicating the filling of biochar pores by TiO_2 nanoparticles [22, 39].

Biochar contained 75.6 wt% C, 1.2 wt% H, 1.5 wt% N, and 21.7 wt% O, with an O/C atomic ratio of 0.22 and an H/C atomic ratio of 0.19. The relatively high O and N contents in biochar could provide abundant
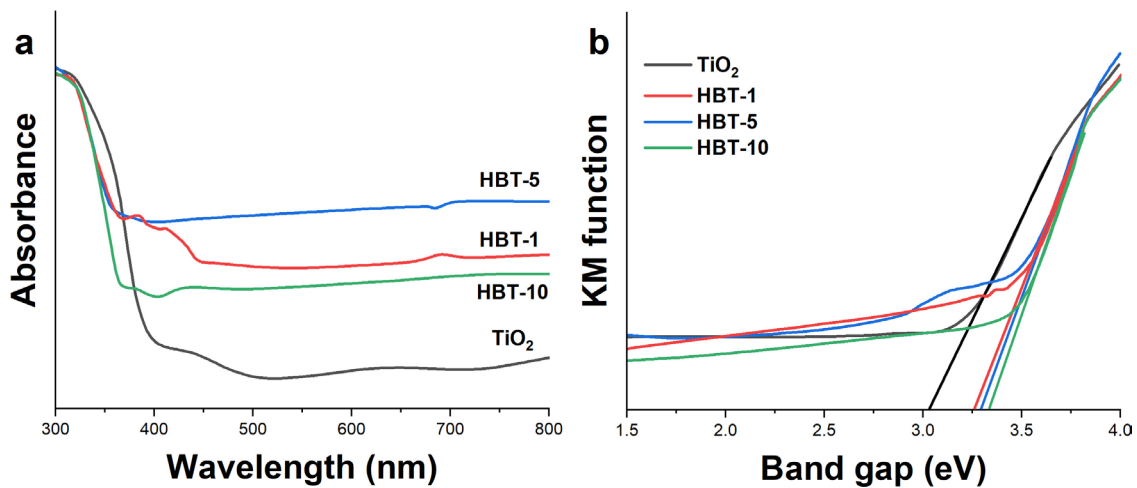

Figure 6: (a) UV-vis diffuse reflectance spectra and (b) Tauc plots of pure TiO_2 and biochar-TiO_2 composites.
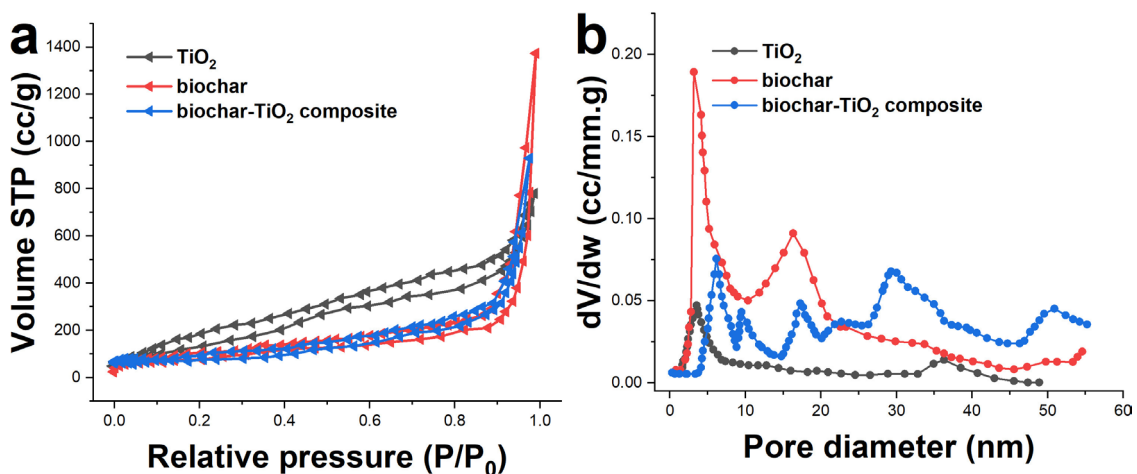

Figure 7: (a) Nitrogen adsorption-desorption isotherms and (b) pore size distribution curves of pure TiO_2, biochar, and biochar-TiO_2 composites.

functional groups for anchoring TiO_2 nanoparticles and enhancing the photocatalytic activity. The hydrothermal method yielded composites with the highest surface areas, pore volumes, and visible light absorption, followed by the solvothermal and mechanical mixing methods. The hydrothermal treatment likely promoted the reduction of oxygen-containing functional groups in biochar and the formation of Ti-O-C bonds, leading to improved interfacial contact and charge transfer between biochar and TiO_2 [40]. Therefore, the hydrothermally prepared HBT-5 composite with 5 wt% biochar content was selected as the optimal photocatalyst for further photocatalytic experiments.

3.2. Photocatalytic performance

The photocatalytic performance of the biochar-TiO_2 composites was evaluated by the removal rate of DCA under UV-vis light irradiation. Figure 8a shows the adsorption and photolysis controls of DCA in the absence of a photocatalyst. Negligible adsorption of DCA was observed on pure biochar in the dark, indicating that the removal of DCA was mainly attributed to photocatalytic degradation rather than adsorption [41]. Under UV-vis light irradiation without a photocatalyst, only 5.2% of DCA was degraded after 180 min, suggesting that direct photolysis of DCA was insignificant.

Figure 8b presents the photocatalytic removal rate of DCA over pure TiO_2 and biochar- TiO_2 composites prepared by different methods. Pure TiO_2 exhibited moderate photocatalytic activity, achieving 45.6% DCA degradation after 180 min. The incorporation of biochar significantly enhanced the photocatalytic performance of TiO_2, with the hydrothermally prepared composites showing the highest activity, followed by the solvothermal and mechanically mixed ones [42]. Among the hydrothermal composites, HBT-5 exhibited the best performance, degrading 92.5% of DCA within 180 min, which was 2.0 and 1.3 times higher than that of pure TiO_2 and HBT-1, respectively. Further increasing the biochar content to 10 wt% (HBT-10) led to a slight decrease in the activity, likely due to the shielding effect of excess biochar on TiO_2 nanoparticles.
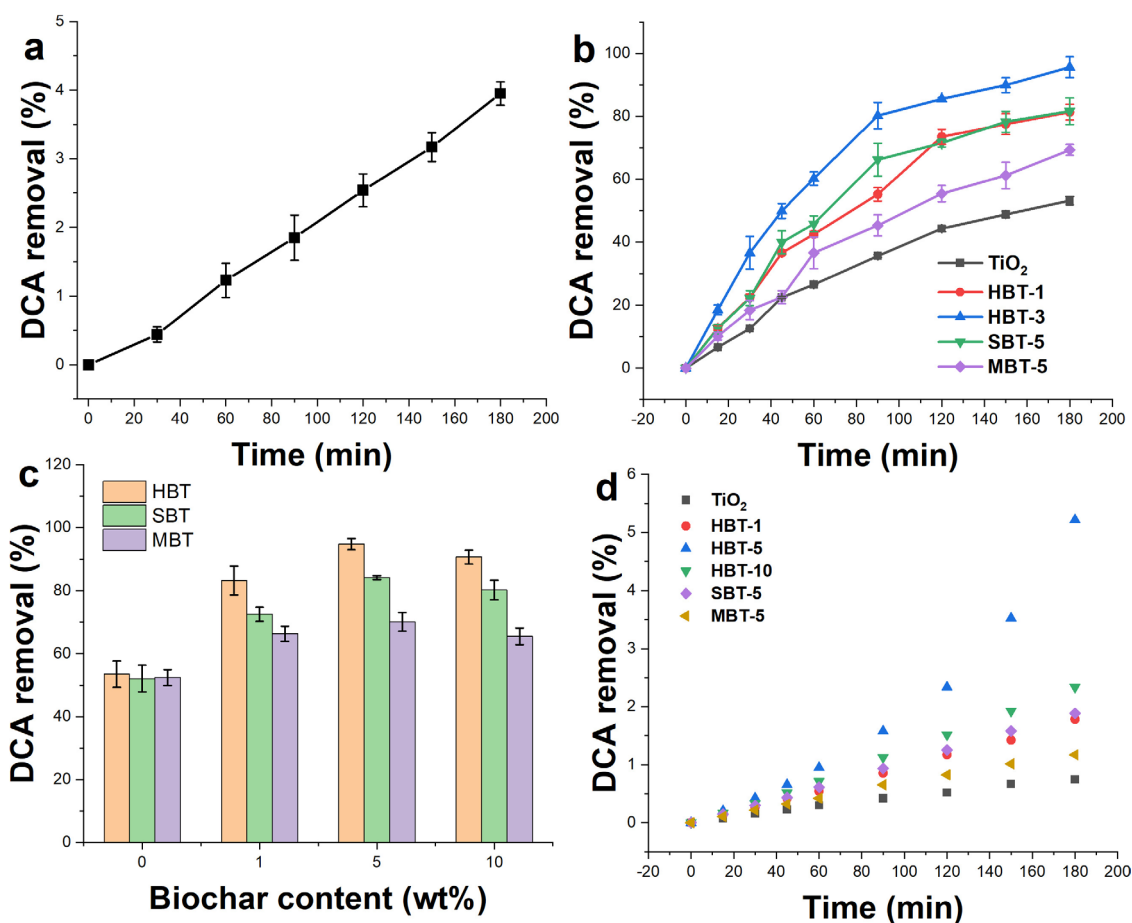

Figure 8: (a) Adsorption and photolysis controls of DCA; (b) Photocatalytic removal rate of DCA over pure TiO_2 and biochar-TiO_2 composites prepared by different methods; (c) Effect of biochar content on the photocatalytic activity of the composites; (d) Pseudo-first-order kinetic plots of DCA removal rate over different photocatalysts.

The effect of biochar content on the photocatalytic activity of the composites was further investigated. As shown in Figure 8c, the removal rate of DCA increased with increasing biochar content from 1 to 5 wt% and then decreased at 10 wt% for all preparation methods. The optimal biochar content was found to be 5 wt%, which provided a balance between the beneficial roles of biochar (e.g., enhanced light absorption, charge separation, and adsorption) and its detrimental effects (e.g., reduced active sites and light scattering). The superior performance of HBT-5 can be attributed to its high surface area, pore volume, and interfacial Ti-O-C bonding, as confirmed by the characterization results [43].

The kinetics of DCA removal rate over the photocatalysts were analyzed using the pseudo-first-order model. The linear plots of $\ln(C_0/C_t)$ versus t are shown in Figure 8d, and the corresponding k values are listed in Table 1. The purpose of Table 1 is to summarize and compare the kinetic parameters of DCA degradation for different photocatalysts, allowing for a quantitative assessment of their performance. This table complements the graphical data presented in Figure 8d and provides a clear, numerical comparison of the photocatalytic efficiency of the various materials tested. The HBT-5 composite exhibited the highest k value of 0.0165 min^{-1}, which was 3.9 and 1.8 times higher than that of pure TiO_2 and HBT-1, respectively. The enhanced photocatalytic activity of HBT-5 can be ascribed to the synergistic effects of biochar and TiO_2, including (i) enhanced light absorption and charge separation due to the sensitization effect of biochar, (ii) improved adsorption and mass transfer of DCA molecules on the porous biochar surface, and (iii) efficient interfacial charge transfer through the Ti-O-C bonding.

The mineralization efficiency of DCA was evaluated by monitoring the TOC removal during the photocatalytic process. As shown in Figure 9a, the TOC removal efficiency followed a similar trend to the DCA removal rate, with HBT-5 achieving the highest mineralization rate of 73.8% after 180 min. The lower TOC removal compared to the DCA removal rate suggests the formation of intermediate products, which were gradually mineralized into CO_2 and H_2O. The mineralization of DCA over HBT-5 was further confirmed by the decreased pH value from 4.5 to 3.2 during the reaction (Figure 9b), indicating the generation of acidic intermediates such as acetic acid and formic acid.

The reusability of the HBT-5 composite was investigated by recycling the photocatalyst for three consecutive runs. As shown in Figure 10, the photocatalytic activity of HBT-5 remained stable, with only a slight

Table 1: Pseudo-first-order rate constants (k) and correlation coefficients (R^2) for DCA degradation over different photocatalysts.

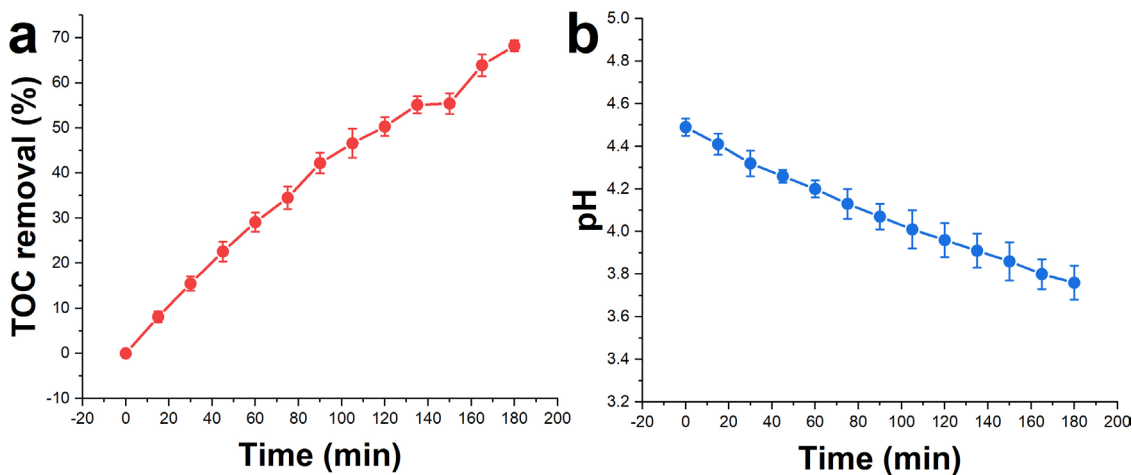| PHOTOCATALYST	k (min^{-1})	R^2
TiO_2	0.0042	0.9923
HBT-1	0.0092	0.9945
HBT-5	0.0165	0.9967
HBT-10	0.0138	0.9958
SBT-5	0.0121	0.9936
MBT-5	0.0078	0.9918

Figure 9: (a) TOC removal efficiency and (b) pH change during the photocatalytic removal rate of DCA over HBT-5.
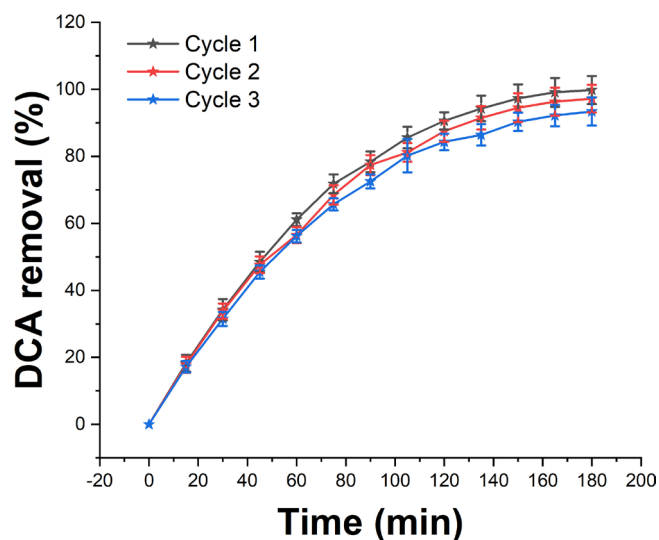
Figure 10: Reusability of HBT-5 for photocatalytic removal rate of DCA over three cycles.

decrease from 92.5% to 87.3% after three cycles. The high stability of HBT-5 can be attributed to the strong interaction between biochar and TiO_2, which prevented the leaching of active components and the aggregation of nanoparticles during the recycling process.

3.3. Mechanisms of enhanced photocatalytic activity

The enhanced photocatalytic activity of the biochar- TiO_2 composites can be attributed to several synergistic effects between biochar and TiO_2, as well as the unique properties of biochar itself. In this section, the roles of biochar in improving charge separation, visible light absorption, and the effects of N and O heteroatoms in biochar are discussed in detail. Firstly, the role of biochar in improving charge separation was investigated by photoluminescence (PL) spectroscopy. Pure TiO_2 exhibited a strong PL emission peak at around 390 nm, which was attributed to the radiative recombination of photogenerated electron-hole pairs. The incorporation of biochar significantly quenched the PL intensity of TiO_2, indicating the suppression of charge recombination [44]. The PL intensity decreased with increasing biochar content, with HBT-5 showing the lowest intensity, which was consistent with its highest photocatalytic activity. The quenching effect of biochar can be ascribed to the efficient transfer of photogenerated electrons from the conduction band of TiO_2 to the biochar surface through the Ti-O-C bonding, as confirmed by the XPS results. The separated electrons on the biochar surface can react with adsorbed O_2 molecules to form reactive oxygen species (ROS), while the holes remain in the valence band of TiO_2 to oxidize DCA directly or indirectly through ROS generation. The conductive carbon network of biochar acts as an electron acceptor, efficiently capturing photogenerated electrons from the TiO_2 conduction band. This process significantly reduces the recombination rate of electron-hole pairs [45], a common limitation in pure TiO_2 photocatalysts. The trapped electrons in the biochar can then participate in redox reactions, such as the reduction of oxygen to form superoxide radicals ($\cdot O_2^-$) [46]. Meanwhile, the holes left in the TiO_2 valence band can directly oxidize DCA molecules or react with water to produce hydroxyl radicals ($\cdot OH$). This spatial separation of charges not only prolongs the lifetime of the photogenerated carriers but also increases the probability of their participation in the degradation reactions [47].

Secondly, the role of biochar in enhancing visible light absorption was studied by UV-vis DRS. Pure TiO_2 only absorbed light in the UV region (< 400 nm) due to its wide bandgap (3.2 eV). The incorporation of biochar extended the light absorption of TiO_2 to the visible region (400–800 nm), which was attributed to the sensitization effect of biochar. The absorption intensity increased with increasing biochar content, with HBT-5 showing the highest visible light absorption. The enhanced visible light absorption of the biochar-TiO_2 composites can be attributed to the narrow bandgap of biochar (1.8 eV) and the formation of Ti-O-C bonds, which can create new electronic states in the bandgap of TiO_2 and facilitate the electron transfer from biochar to TiO_2 under visible light irradiation. The photocurrent response of the composites under visible light irradiation further confirmed the enhanced visible light activity of the biochar-TiO_2 composites, with HBT-5 showing the highest photocurrent density of 2.5 $\mu A/cm^2$, which was 3.1 times higher than that of pure TiO_2.

Thirdly, the effect of N and O heteroatoms in biochar on the photocatalytic activity of the composites was investigated. As confirmed by the XPS results, biochar contained a significant amount of N (1.5 wt%) and

O (21.7 wt%) heteroatoms, which could serve as electron donors and acceptors, respectively, to modify the electronic structure of biochar. The high-resolution N1s XPS spectrum of biochar revealed the presence of three types of N species: pyridinic-N (398.5 eV), pyrrolic-N (400.1 eV), and graphitic-N (401.3 eV). Among them, pyridinic-N and graphitic-N are reported to be more effective in promoting the photocatalytic activity of TiO_2 by enhancing the electron transfer and visible light absorption. The high-resolution O 1s XPS spectrum of biochar showed three types of O species: C=O (531.2 eV), C-O (532.5 eV), and O-H (533.5 eV). The C=O and C-O groups can act as electron acceptors to trap the photogenerated electrons from TiO_2, while the O-H groups can facilitate the adsorption of water molecules and the generation of hydroxyl radicals.

4. CONCLUSION

In summary, this study successfully synthesized novel nano-biochar supported TiO_2 composites using different methods (hydrothermal, solvothermal, and mechanical) and biochar/TiO_2 ratios (1–10%) for the effective removal of DCA from swimming pool water. Comprehensive characterization techniques confirmed the strong interaction and synergistic effects between biochar and TiO_2, with the hydrothermally prepared HBT-5 composite (5 wt% biochar) exhibiting the highest photocatalytic activity, degrading 92.5% of DCA within 180 min under UV-vis light irradiation, which was 2.0 and 1.3 times higher than that of pure TiO_2 and HBT-1, respectively. The enhanced performance of HBT-5 was attributed to its high surface area, pore volume, interfacial Ti-O-C bonding, enhanced visible light absorption, efficient charge separation, and the presence of N and O heteroatoms in biochar. The photocatalyst also showed excellent reusability, maintaining 87.3% of its initial activity after three cycles. This work provides new insights into the design and application of biochar-based photocatalysts for water purification, with potential benefits for public health and environmental protection.

5. BIBLIOGRAPHY

[1]   MANASFI, T., COULOMB, B., BOUDENNE, J.-L., "Occurrence, origin, and toxicity of disinfection byproducts in chlorinated swimming pools: an overview", *International Journal of Hygiene and Environmental Health*, v. 220, n. 3, pp. 591–603, May 2017. doi: http://doi.org/10.1016/j.ijheh.2017.01.005. PubMed PMID: 28174041.

[2]   ILYAS, H., MASIH, I., VAN DER HOEK, J.P., "Disinfection methods for swimming pool water: byproduct formation and control", *Water*, v. 10, n. 6, pp. 797, Jun. 2018. doi: http://doi.org/10.3390/w10060797.

[3]   SKIBINSKI, B., UHLIG, S., MÜLLER, P., *et al*., "Impact of different combinations of water treatment processes on the concentration of disinfection byproducts and their precursors in swimming pool water", *Environmental Science & Technology*, v. 53, n. 14, pp. 8115–8126, Jul. 2019. doi: http://doi.org/10.1021/acs.est.9b00491. PubMed PMID: 31180210.

[4]   WANG, J., GONG, T., XIAN, Q., "Formation of haloacetic acids from different organic precursors in swimming pool water during chlorination", *Chemosphere*, v. 247, pp. 125793, May 2020. doi: http://doi.org/10.1016/j.chemosphere.2019.125793. PubMed PMID: 31931310.

[5]   ZHAO, H., YANG, L., LI, Y., *et al*., "Environmental occurrence and risk assessment of haloacetic acids in swimming pool water and drinking water", *RSC Advances*, v. 10, n. 47, pp. 28267–28276, 2020. doi: http://doi.org/10.1039/D0RA02389B. PubMed PMID: 35519123.

[6]   YANG, L., CHEN, X., SHE, Q., *et al*., "Regulation, formation, exposure, and treatment of disinfection by-products (DBPs) in swimming pool waters: a critical review", *Environment International*, v. 121, n. Pt 2, pp. 1039–1057, Dec. 2018. doi: http://doi.org/10.1016/j.envint.2018.10.024. PubMed PMID: 30392941.

[7]   HAMA AZIZ, K.H., "Application of different advanced oxidation processes for the removal of chloroacetic acids using a planar falling film reactor", *Chemosphere*, v. 228, pp. 377–383, Aug. 2019. doi: http://doi.org/10.1016/j.chemosphere.2019.04.160. PubMed PMID: 31042611.

[8]   BELTRÁN, F.J., REY, A., GIMENO, O., "The role of catalytic ozonation processes on the elimination of dbps and their precursors in drinking water treatment", *Catalysts*, v. 11, n. 4, pp. 521, Apr. 2021. doi: http://doi.org/10.3390/catal11040521.

[9]   SIDDIQUE, M.S., XIONG, X., YANG, H., *et al*., "Dynamic variations in DOM and DBPs formation potential during surface water treatment by ozonation-nanofiltration: Using spectroscopic indices approach", *Chemical Engineering Journal*, v. 427, pp. 132010, Jan. 2022. doi: http://doi.org/10.1016/j.cej.2021.132010.

[10] WANG, L., CHEN, Y., CHEN, B., *et al*., "Generation of hydroxyl radicals during photodegradation of chloroacetic acids by 254 nm ultraviolet: A special degradation process revealed by a holistic radical

determination methodology", *Journal of Hazardous Materials*, v. 404, n. Pt B, pp. 124040, Feb. 2021. doi: http://doi.org/10.1016/j.jhazmat.2020.124040. PubMed PMID: 33157519.

[11] DHARMA, H.N.C., JAAFAR, J., WIDIASTUTI, N., *et al*., "A review of titanium dioxide (TiO2)-based photocatalyst for oilfield-produced water treatment", *Membranes*, v. 12, n. 3, pp. 345, Mar. 2022. doi: http://doi.org/10.3390/membranes12030345. PubMed PMID: 35323821.

[12] KUSIAK-NEJMAN, E., MORAWSKI, A.W., "TiO2/graphene-based nanocomposites for water treatment: a brief overview of charge carrier transfer, antimicrobial and photocatalytic performance", *Applied Catalysis B: Environmental*, v. 253, pp. 179–186, Sep. 2019. doi: http://doi.org/10.1016/j.apcatb.2019.04.055.

[13] AWFA, D., ATEIA, M., FUJII, M., *et al*., "Photodegradation of pharmaceuticals and personal care products in water treatment using carbonaceous-TiO2 composites: a critical review of recent literature", *Water Research*, v. 142, pp. 26–45, Oct. 2018. doi: http://doi.org/10.1016/j.watres.2018.05.036. PubMed PMID: 29859390.

[14] RIAZ, S., PARK, S.-J., "An overview of TiO2-based photocatalytic membrane reactors for water and wastewater treatments", *Journal of Industrial and Engineering Chemistry*, v. 84, pp. 23–41, Apr. 2020. doi: http://doi.org/10.1016/j.jiec.2019.12.021.

[15] AL-MAMUN, M.R., KADER, S., ISLAM, M.S., *et al*., "Photocatalytic activity improvement and application of UV-TiO$_2$ photocatalysis in textile wastewater treatment: a review", *Journal of Environmental Chemical Engineering*, v. 7, n. 5, pp. 103248, Oct. 2019. doi: http://doi.org/10.1016/j.jece.2019.103248.

[16] WANG, W., ZHANG, J., CHEN, T., *et al*., "Preparation of TiO$_2$-modified biochar and its characteristics of photo-catalysis degradation for enrofloxacin", *Scientific Reports*, v. 10, n. 1, pp. 6588, Apr. 2020. doi: http://doi.org/10.1038/s41598-020-62791-5. PubMed PMID: 32313014.

[17] CHANDRA, S., JAGDALE, P., MEDHA, I., *et al*., "Biochar-supported TiO$_2$-based nanocomposites for the photocatalytic degradation of sulfamethoxazole in water—a review", *Toxics*, v. 9, n. 11, pp. 313, Nov. 2021. doi: http://doi.org/10.3390/toxics9110313. PubMed PMID: 34822704.

[18] FAZAL, T., RAZZAQ, A., JAVED, F., *et al*., "Integrating adsorption and photocatalysis: a cost effective strategy for textile wastewater treatment using hybrid biochar-TiO2 composite", *Journal of Hazardous Materials*, v. 390, pp. 121623, May 2020. doi: http://doi.org/10.1016/j.jhazmat.2019.121623. PubMed PMID: 31753670.

[19] SILVA, C.P., PEREIRA, D., CALISTO, V., *et al*., "Biochar-TiO$_2$ magnetic nanocomposites for photocatalytic solar-driven removal of antibiotics from aquaculture effluents", *Journal of Environmental Management*, v. 294, pp. 112937, Sep. 2021. doi: http://doi.org/10.1016/j.jenvman.2021.112937. PubMed PMID: 34119993.

[20] XIE, Y., LIU, A., BANDALA, E.R., *et al*., "TiO$_2$-biochar composites as alternative photocatalyst for stormwater disinfection", *Journal of Water Process Engineering*, v. 48, pp. 102913, Aug. 2022. doi: http://doi.org/10.1016/j.jwpe.2022.102913.

[21] GUO, D., FENG, D., ZHANG, Y., *et al*., "Synergistic mechanism of biochar-nano TiO2 adsorption-photocatalytic oxidation of toluene", *Fuel Processing Technology*, v. 229, pp. 107200, May 2022. doi: http://doi.org/10.1016/j.fuproc.2022.107200.

[22] LI, D., FANG, Y., LU, J., *et al*., "Enhanced biodegradation of PAHs by biochar and a TiO$_2$@biochar composite under light irradiation: Photocatalytic mechanism, toxicity evaluation and ecological response", *Chemical Engineering Journal*, v. 458, pp. 141495, Feb. 2023. doi: http://doi.org/10.1016/j.cej.2023.141495.

[23] DE MORAES, N.P., BACETTO, L.A., GOES, C.M., *et al*., "Desenvolvimento de compósitos ZnC$_2$O$_4$/xerogel de carbono para degradação fotocatalítica de azul de metileno sob radiação solar", *Matéria (Rio de Janeiro)*, v. 26, n. 2, pp. e12998, May 2021. doi: http://doi.org/10.1590/s1517-707620210002.12998.

[24] DE SOUSA, J.G.M., DE MORAES, N.P., GOES, C.M., *et al*., "Avaliação das propriedades estruturais e fotocatalíticas de compósitos g-C$_3$N$_4$/ZnO/xerogel de carbono sintetizados com diferentes tipos de tanino", *Matéria (Rio de Janeiro)*, v. 27, n. 1, pp. e13131, May 2022. doi: http://doi.org/10.1590/s1517-707620220001.1331.

[25] CAI, X., LI, J., LIU, Y., *et al*., "Titanium dioxide-coated biochar composites as adsorptive and photocatalytic degradation materials for the removal of aqueous organic pollutants", *Journal of Chemical Technology and Biotechnology (Oxford, Oxfordshire)*, v. 93, n. 3, pp. 783–791, 2018. doi: http://doi.org/10.1002/jctb.5428.

[26] FENG, X., LI, X., SU, B., *et al.*, "Solid-phase fabrication of TiO$_2$/Chitosan-biochar composites with superior UV-vis light driven photocatalytic degradation performance", *Colloids and Surfaces. A, Physicochemical and Engineering Aspects*, v. 648, pp. 129114, Sep. 2022. doi: http://doi.org/10.1016/j.colsurfa.2022.129114.

[27] QU, K., HUANG, L., HU, S., *et al.*, "TiO2 supported on rice straw biochar as an adsorptive and photocatalytic composite for the efficient removal of ciprofloxacin in aqueous matrices", *Journal of Environmental Chemical Engineering*, v. 11, n. 2, pp. 109430, Apr. 2023. doi: http://doi.org/10.1016/j.jece.2023.109430.

[28] LU, L., SHAN, R., SHI, Y., *et al.*, "A novel TiO$_2$/biochar composite catalysts for photocatalytic degradation of methyl orange", *Chemosphere*, v. 222, pp. 391–398, 2019. doi: http://doi.org/10.1016/j.chemosphere.2019.01.132. PubMed PMID: 30711728.

[29] YU, Y., LIU, S., WANG, W., *et al.*, "Eco-friendly utilization of sawdust: Ionic liquid-modified biochar for enhanced Li+ storage of TiO$_2$", *The Science of the Total Environment*, v. 794, pp. 148688, Nov. 2021. doi: http://doi.org/10.1016/j.scitotenv.2021.148688. PubMed PMID: 34218152.

[30] EL-AZAZY, M., EL-SHAFIE, A.S., MORSY, H., "Biochar of spent coffee grounds as per Se and impregnated with TiO$_2$: promising waste-derived adsorbents for balofloxacin", *Molecules*, v. 26, n. 8, pp. 2295, Jan. 2021. doi: http://doi.org/10.3390/molecules26082295. PubMed PMID: 33921054.

[31] ABODIF, A.M., MENG, L., MA, S., *et al.*, "Mechanisms and models of adsorption: TiO$_2$-supported biochar for removal of 3,4-dimethylaniline", *ACS Omega*, v. 5, n. 23, pp. 13630-13640, Jun. 2020. doi: http://doi.org/10.1021/acsomega.0c00619. PubMed PMID: 32566828.

[32] LAZAROTTO, J.S., DE LIMA BROMBILLA, V., SILVESTRI, S., *et al.*, "Conversion of spent coffee grounds to biochar as promising TiO2 support for effective degradation of diclofenac in water", *Applied Organometallic Chemistry*, v. 34, n. 12, pp. e6001, 2020. doi: http://doi.org/10.1002/aoc.6001.

[33] CASTILLA-CABALLERO, D., HERNANDEZ-RAMIREZ, A., VAZQUEZ-RODRIGUEZ, S., *et al.*, "Effect of pyrolysis, impregnation, and calcination conditions on the physicochemical properties of TiO$_2$/Biochar composites intended for photocatalytic applications", *Journal of Environmental Chemical Engineering*, v. 11, n. 3, pp. 110274, Jun. 2023. doi: http://doi.org/10.1016/j.jece.2023.110274.

[34] SHA, J., SUN, Y., YU, H., *et al.*, "Comparison of nano-TiO$_2$ immobilization approaches onto biochar: superiorities of click chemistry strategy and self-acceleration of pollutant degradation", *Journal of Environmental Chemical Engineering*, v. 10, n. 3, pp. 107544, Jun. 2022. doi: http://doi.org/10.1016/j.jece.2022.107544.

[35] CHEN, X.-L., LI, F., CHEN, H., *et al.*, "Fe$_2$O$_3$/TiO$_2$ functionalized biochar as a heterogeneous catalyst for dyes degradation in water under Fenton processes", *Journal of Environmental Chemical Engineering*, v. 8, n. 4, pp. 103905, Aug. 2020. doi: http://doi.org/10.1016/j.jece.2020.103905.

[36] WANG, T., MENG, Z., SHENG, L., *et al.*, "Insights into the mechanism of co-adsorption between tetracycline and nano-TiO$_2$ on coconut shell porous biochar in binary system", *Advanced Powder Technology*, v. 32, n. 11, pp. 4120–4129, Nov. 2021. doi: http://doi.org/10.1016/j.apt.2021.09.014.

[37] MOHTARAM, M.S., MOHTARAM, S., SABBAGHI, S., *et al.*, "Photocatalytic degradation of acetaminophen using a novel TiO$_2$-orange peel-derived biochar composite: synthesize, characterization and optimization of key factors", *Journal of Water Process Engineering*, v. 58, pp. 104884, Feb. 2024. doi: http://doi.org/10.1016/j.jwpe.2024.104884.

[38] SHI, J., HUANG, W., ZHU, H., *et al.*, "Facile fabrication of durable biochar/H$_2$-TiO$_2$ for highly efficient solar-driven degradation of enrofloxacin: properties, degradation pathways, and mechanism", *ACS Omega*, v. 7, n. 14, pp. 12158–12170, Apr. 2022. doi: http://doi.org/10.1021/acsomega.2c00523. PubMed PMID: 35449975.

[39] ESCAMILLA-MEJÍA, J.C., HIDALGO-CARRILLO, J., MARTÍN-GÓMEZ, J., *et al.*, "Biochars from olive stones as carbonaceous support in Pt/TiO$_2$-carbon photocatalysts and application in hydrogen production from aqueous glycerol photoreforming", *Nanomaterials*, v. 13, n. 9, pp. 1511, Jan. 2023. doi: http://doi.org/10.3390/nano13091511. PubMed PMID: 37177056.

[40] ZHOU, X., ZHU, Y., NIU, Q., *et al.*, "New notion of biochar: a review on the mechanism of biochar applications in advannced oxidation processes", *Chemical Engineering Journal*, v. 416, pp. 129027, Jul. 2021. doi: http://doi.org/10.1016/j.cej.2021.129027.

[41] MEEPHON, S., RUNGROTMONGKOL, T., PUTTAMAT, S., *et al.*, "Heterogeneous photocatalytic degradation of diuron on zinc oxide: Influence of surface-dependent adsorption on kinetics, degradation

pathway, and toxicity of intermediates", *Journal of Environmental Sciences*, v. 84, pp. 97–111, Oct. 2019. doi: http://doi.org/10.1016/j.jes.2019.04.016. PubMed PMID: 31284920.

[42] RIVERO, M.J., RIBAO, P., GOMEZ-RUIZ, B., *et al*., "Comparative performance of TiO$_2$-rGO photocatalyst in the degradation of dichloroacetic and perfluorooctanoic acids", *Separation and Purification Technology*, v. 240, pp. 116637, Jun. 2020. doi: http://doi.org/10.1016/j.seppur.2020.116637.

[43] ZHONG, J., ZHAO, Y., DING, L., *et al*., "Opposite photocatalytic oxidation behaviors of BiOCl and TiO$_2$: direct hole transfer vs. indirect OH oxidation", *Applied Catalysis B: Environmental*, v. 241, pp. 514–520, Feb. 2019. doi: http://doi.org/10.1016/j.apcatb.2018.09.058.

[44] WANG, W., YANG, R., LI, T., *et al*., "Advances in recyclable and superior photocatalytic fibers: Material, construction, application and future perspective", *Composites. Part B, Engineering*, v. 205, pp. 108512, Jan. 2021. doi: http://doi.org/10.1016/j.compositesb.2020.108512.

[45] BERTUZZO, V.L., DE CARVALHO NETO, A.V., DOS SANTOS, D.I., "Síntese Conjunta do compósito nanoestruturado Fe$_2$O$_3$-SnO$_2$ pelo método poliol e seu desempenho fotocatalítico no descoramento da rodamina-B", *Matéria (Rio de Janeiro)*, v. 28, n. 1, pp. e20220180, Feb. 2023. doi: http://doi.org/10.1590/1517-7076-rmat-2022-0180.

[46] WANG, Y., DING, K., XU, R., *et al*., "Fabrication of BiVO$_4$/BiPO$_4$/GO composite photocatalytic material for the visible light-driven degradation", *Journal of Cleaner Production*, v. 247, pp. 119108, Feb. 2020. doi: http://doi.org/10.1016/j.jclepro.2019.119108.

[47] ZHANG, H., YU, D., WANG, W., *et al*., "Recyclable and highly efficient photocatalytic fabric of Fe(III)@BiVO$_4$/cotton via thiol-ene click reaction with visible-light response in water", *Advanced Powder Technology*, v. 30, n. 12, pp. 3182–3192, Dec. 2019. doi: http://doi.org/10.1016/j.apt.2019.09.027.